MAIA S2 Versus Sentinel 2: Spectral Issues and Their Effects in the Precision Farming Context

Filippo Sarvia(✉), Samuele De Petris, Tommaso Orusa, and Enrico Borgogno-Mondino

DISAFA, University of Torino, L-go Braccini 2, 10095 Grugliasco, TO, Italy
Filippo.sarvia@unito.it

Abstract. Precision agriculture involves the integration of new technologies including Geographic Information Systems (GIS), Global Navigation Satellites Systems (GNSS) and Remote Sensing (RS) platforms and sensors to allow farmers to maximize the cost-benefit ratio, rather than using the traditional whole-field approach. MAIA S2 is a recent multispectral aerial sensor in strong expansion in the agricultural sector. In this work, MAIA S2 spectral properties were compared with the correspondent Sentinel-2 ones, focusing on possible effects that differences could induce onto agriculture related deductions. The reference dataset was acquired by aerial survey and radiometric and geometric pre-processing achieved to generate the correspondent at-the-ground reflectance multispectral orthomosaic by ordinary workflow as suggested by sensor suppliers. A comparison was achieved at single band level to test spectral consistency of the two data. It showed a low correlation in the red-edge and infrared bands ($r < 0.5$); oppositely, a higher correlation was found for the visible bands ($r > 0.8$). To test the effects of found discrepancies between the two data, the correspondent prescription maps were generated using the same clustering criterion. They were then compared to test consistency of deductions.

Keywords: Precision agriculture · MAIA S2 sensor · Sentinel-2 · Precision farming · Prescription maps · MAIA S2 radiometric accuracy

1 Introduction

1.1 Precision Agriculture Requirements and Expected Applications

Precision agriculture, better defined as technological agriculture, involves the integration of new technologies including Geographic Information Systems (GIS), Global Navigation Satellites Systems (GNSS) and Remote Sensing (RS) platforms and sensors with the aim of making farmers able to better manage within field variability and maximize the cost-benefit ratio. Variable Rate Technology (VRT) available for many machineries, such as fertilizers or pesticide applicators and yield monitors, has evolved rapidly and have fostered the technological agriculture (TA) [1]. RS provides input data for many applications including pre-growth soil fertility and moisture analyses, crop growth and yield

© Springer Nature Switzerland AG 2021
O. Gervasi et al. (Eds.): ICCSA 2021, LNCS 12955, pp. 63–77, 2021.
https://doi.org/10.1007/978-3-030-87007-2_5

forecasting [2]. This information helps the farmer in his decision-making. Nevertheless, in spite of its fame, precision agriculture still suffers from many lacks/weaknesses to be effectively retained as fully operational. With special concerns about RS, some important issues are still to be completely clarified concerning both radiometric and geometric requirements. The unprecedented availability of satellite images guaranteeing proper spatial, spectral and temporal resolutions, has promoted the use of remote sensing in many TA applications [3] like crop monitoring, crop insurance [4–6], irrigation management, tree stability assessment [7, 8], nutrient application, Common Agricultural Policy controls [9], disease and pest management, natural hazards monitoring [10–12], assessment of climate change effects on vegetation [13], wildlife disease assessment [14], and yield prediction [15, 16]. In spite of these applications airborne multispectral sensor were greatly involved in TA. This work focuses on the comparison between Copernicus Sentinel 2 data (hereinafter called S2) and those acquired by the MAIA S2 (hereinafter called MS2, SAL Engineering s.r.l.) during a flight operated by airplane over an agricultural landscape contemporarily to the S2 passage. The comparison was specifically addressed to highlight spectral differences trying to figure out possible consequences in TA related deductions. The main issue concerned the evaluation of the spectral consistency between the two dataset and the eventual operational consequences that differences can generate in intepretating the data.

1.2 Multispectral Sensors in TA

RS solutions used for TA, can be classified in function of: (i) sensor platform and (ii) type of sensor. Sensors are typically mounted on board of satellite, aerial, and ground-based platforms. From the 1970s, satellite technology and products were widely used for TA. Recently, airborne systems including aircraft and RPAS (Remotely Piloted Aerial Vehicle) are also being used in TA. Ground-based platforms adopted in TA can be classified into three classes: (i) hand-held, (ii) free standing in the field, and (iii) mounted on tractor or farm machinery. Ground-based solutions are referred to as proximal RS systems since they are located closer to the target surfaces (terrain or plants). Multispectral sensors seem to play a particular role, given the whole of applications they can be suitable for [17]. RS Sensors differ for spatial, spectral, radiometric, and temporal resolution [18–20]. Aerial platforms generally provide higher spatial resolution (today often lower than 1 m) and a great productivity making them more desirable than satellites when moving the analysis within the single field. Nevertheless, the significantly improved temporal, spatial, and spectral resolution of the European Space Agency (ESA) Copernicus Sentinel-2 A/B twin platform is paving the way to their popularization in TA.

1.3 MAIA S2 Sensor

A wide selection of multispectral imaging sensors are currently offered on the market, most of them designed to be placed on various platform, in particular on airplanes or small drones. MAIA S2 [21] was developed to be preferably used on RPAS, but recent experiences have demonstrated that it could be also used from airplane flying at AGL (Above Ground Level) height higher than 250 m. MS2 can acquire the VIS-NIR spectral range (390–950 nm), running at a frame rate of up 6 Hz per sensor [1]. All sensors (one

for each band, Table 1) is equipped with a calibrated bandpass filter. The nine band-pass filters that are installed in the MS2 camera have the identical central wavelength and bandwidth as those implemented by the MSI (Multi Spectral Instrument) of S2 [18].

MS2 sensor [18] was used for all the acquisitions having the following technical features: focal length = 7.5 mm, physical pixel size = 3.75 μm, sensor size = 1280 × 960 pixels.

It is expected that MS2 and S2 data could be efficiently integrated for analysis downscaling in the agricultural field [22].

Table 1. Nominal technical features of MAIA S2 sensor.

MAIA/S2			
Bands (MS2, S2)	Central wavelength (nm)	Bands width (nm)	Spectral region
b1, b1	443	20	Violet
b2, b2	490	65	Blue
b3, b3	560	35	Green
b4, b4	665	30	Red
b5, b5	705	15	Red Edge 1
b6, b6	740	15	Red Edge 2
b7, b7	783	20	NIR 1
b8, b8	842	115	NIR 2
b9, b8a	865	20	NIR 3

In MS2, acquisition settings, such as the exposure time and acquisition frame rate, may be adjusted through the user's interface to suit specific work conditions. Images are recorded on an internal solid state hard disk (SSD), which can store more than 10,000 RAW images. Images were stored in a proprietary RAW format where the radiometric resolution can be configured to 8, 10 or 12 bits. Camera settings can be accessed by user through the proprietary software making possible to (i) configure the parameters, (ii) visualize a live preview during the acquisition and (iii) capture and store the selected images to the internal storage. Several interfaces are available for these purposes: the keyboard control, NTSC/PAL video output, a web panel, and 2 inputs for remote controllers. Remote control can be accessed via a high-speed GigaEthernet connection or WiFi connection to a tablet, personal computer or smartphone, which can be convenient when used in the field. Finally, the MS2 camera can be connected with other sensors:

– a radio transmitter to transmit the images to the user for real-time monitoring;
– a gimbal controlled by the sensor inertial within the camera in order to maintain a constant or adapt the sensor posture during flight;
– a remote controller to modify certain parameters manually during the flight;
– an external GNSS receiver to geo-tag the images;

– other devices that may provide or need a precise synchronization signal at the same moment of image exposure.

The system is completed with the Irradiance Light Sensor (ILS) that was mounted on the upper part of the aerial fuselage. ILS operates with the same CMOS sensor of MS2 and is devoted to measure Sun irradiance in the same bands as MS2.

2 Materials and Methods

2.1 Study Area

An area of interest (AOI) was selected within the province of Vercelli (NW-Italy) having a size of about 166 ha (Fig. 1). AOI is mainly characterized by an agricultural landscape where corn, grassland and wheat represent the most important crops. In particular, to evaluate the effects of inconsistencies on prescription maps obtained from the two sensors, a focus area (FA), covering a corn field (about 7.2 ha), was selected.



Fig. 1. Study area. Area of interest (red). Focus area covering a corn field (yellow). Reference system is WGS 84 UTM zone 32 N, EPSG: 32632 (Color figure online).

2.2 Available Data

An aerial survey was performed on 6th August 2020 from a Tecnam P92 JS airplane. Forward and side overlap were set equal to 82% and 87% respectively and the aerial survey was performed @ 600 m AGL. MS2 sensor was hosted in the SkyMetry©/SmartBay© platform by Digisky s.r.l. company [23].

Image block was adjusted using 6 ground control points (GCPs, Fig. 2). GCPs were collimated from available high resolution orthoimages (planimetric coordinates) and DTM (height coordinate) in order to reduce costs and speed up the process. The reference true color orthoimage was produced by the TeA Consortium in summer 2015 with a Ground Sampling Distance (GSD) equal to 0.40 m and georeferenced in the WGS84 UTM 32 reference frame. GCP height coordinate was obtained from the Piemonte Region digital terrain model (DTM, Ground Sample Distance = 5 m, height accuracy = 0.33 m).

These data were obtained for free from the regional Geoportal (www.geoportale.piemonte.it). GCPs were selected in correspondence of well recognizable features like road crossings, houses corners, backhoes, plinths, etc.



Fig. 2. Number and position of ground control points. Reference system is WGS 84 UTM zone 32 N, EPSG: 32632.

Multispectral satellite data from the Copernicus Sentinel-2 mission [24] were used to test spectral quality of MS2 multispectral acquisitions. A S2 Level-2A image acquired on 7th August 2020 (one day later of MS2 acquisition) was obtained from the official European Space Agency data hub (ESA, https://scihub.copernicus.eu/). It is worth to remind that a S2 tile covers an area of 100 $\times$ 100 km^2 and is supplied projected in the WGS84 UTM reference system. Level 2A imagery is provided calibrated in at-the-ground reflectance (Bottom of the Atmosphere, BOA) [25] making it immediately suitable for terrestrial applications.

2.3 Data Processing

MS2 Data Pre-processing. Acquired raw images were processed by the MAIA proprietary software named MultiCam Stitcher Pro v 1.4-Beta 2 (MCS). Initially, images were geometrically corrected to remove/minimize distortions related to sensor lens system and design using the available automatic procedure in MCS. Nominal calibration parameters, different for each band, are recorded within MCS and automatically applied during processing [17]. Successively, a co-registration step aiming at aligning bands (since acquired from different lens systems) was achieved by MCS. A block made of multi-layer images containing 9 co-registered and undistorted bands was therefore generated. Data from MS2 were quantized at 12 bits and saved as integer numbers at 2 bytes (16 bits) determining a range of variation between 0 and 65520. Radiometric calibration, aimed at recovering reflectance from DN, was achieved again using the automatic

procedure available in MSC based on the measurement of Sun irradiance as coming from ILS. The calibration approach assumes that the incoming radiation measured by ILS corresponds to the same that lights the scene recorded by MS2. This is, obviously, a significant simplification that does not consider topographic effect during reflectance computation, assuming the same value for all the band pixels. Reflectance is obtained by MCS by (1).

$$\rho_{\lambda}^{i} = \frac{1}{ILS_{\lambda}} DN_{\lambda}^{i} \tag{1}$$

where ILS_{λ} is the 12 bits quantized value of irradiance detected by ILS for the λ spectral band and the *i*-th pixel of the image; DN_{λ}^{i} is the 12 bits quantized DN of the *i*-th pixel of band λ. Since ρ_{λ}^{i} is saved in the output multispectral calibrated image as 2 byte unsigned integer, to recover expected reflectance values from calibrated data user is called to divide them by 65520 (as suggested by SAL Engineering technical personnel). From an operational point of view this appears a weakness of the proposed approach especially when the software is used by unskilled people. It also appears strange that the 65520 value is used at this step (when quantization problem has been already solved by ratio (1)) in place of the expected value of 65535 (16 bits upper bound). Moreover the parameters applied during the "Crop M-Layer Tiff" phase, required by the MCS software, were set: 30; 881; 49 and 1206 pixels for the top, bottom, left and right borders respectively. This approach, following the standard workflow as suggested by the software, moves data from the rigorous conditions required by ordinary photogrammetric processes. In fact, an asymmetric crop of image is expected to shift the fiducial centre of images, making interior orientation parameters potentially wrong. At this point it is not clear the effects of such strategy during image bundle adjustment. We also expect that radiometric radial distortions could be somehow affected [26]. Some further investigations have still to be done.

MS2 Data Bundle Adjustment. The radiometrically calibrated image block was then processed by Agisoft PhotoScan vs 1.2.4 software (AGS) to solve images orientation (bundle adjustment) needed to generate the multispectral orthomosaic (MOM). It is worth to remind that AGS operates according to the Structure-from-Motion (SfM) approach to estimate exterior and, eventually, interior orientation parameters of images and makes possible the generation of a photogrammetric point cloud (PPC) with a proper reference system (WGS84 UTM 32N for this work). During block adjustment 6 GCPs were collimated on reference data. Obtained PPC was therefore filtered to remove outliers and the correspondent Digital Surface Model (DSM) computed by regularization setting a GSD of 1.2 m. A leave-one out (LOO) procedure [27] was adopted to test bundle adjustment accuracy. Altimetric and planimetric RMSE (Root Mean Squared Error) were computed. Finally, MOM having a GSD of 0.3 m was generated using the above mentioned DSM from the calibrated multispectral images. While mosaicking images blending mode was set to "disabled" to not further move native radiometry of calibrated images.

MAIA S2 and S2 Comparison

Band Spectral Correlation. In order to test MS2 and S2 spectral consistency, the temporally closest S2 acquisition was used as reference. It is worth to remind that S2 imagery is provided already calibrated in at-the-ground reflectance by Copernicus SciHub provider and represents a sort of standard to compare other sensors reflectances with. MS2 image was preliminary down-sampled to the same S2 geometric resolution (10 m) adopting the mean method [28]. Subsequently, correspondent bands from MS2 and S2 were compared and relationship modeled by I order polynomial regression. Correspondent gain, offset, Pearson's r and coefficient of determination (R^2) were computed.

Spectral Signature Comparison. Starting from the down-sampled MOM spectral signatures were compared at pixel level. Pearson's *r* and Mean Absolute Error (MAE) [29] were calculated and mapped into separate layers hereafter called *r* map (RM) and MAE map (MM) respectively.

Vegetation Index Comparison. MS2 is extensively adopted for agricultural purposes [18, 30]. The majority of works involving MS2 use spectral vegetation indices (NDVI, Normalized Difference Vegetation Index or NDRE, Normalized Difference Red Edge Index) as predictors to base agronomic deductions on (e.g. prescription map generation). With special focus on NDVI, authors compared resulting maps from MS2 and S2 datasets, hereinafter called $NDVI_{MS2}$ and $NDVI_{S2.}$ With reference to the standard deviation of both NDVI maps, a F-test was performed to test the hypothesis that the two NDVI variances were significantly different. Additionally, a I order polynomial regression was calibrated between $NDVI_{MS2}$ and $NDVI_{S2}$ and correspondent gain, offset, Pearson's r and coefficient of determination computed.

Effects of Differences on Precision Farming Products. It is worth to remind that in the precision agriculture context spectral measures inconsistencies can drive to different deductions making probable that wrong agricultural practices are adopted [31]. To test this condition, an assessment about consistency of MS2 and S2 derived prescription maps was performed. To map behavioral zones within a test field (FA) an approach based on the cluster analysis was adopted. Several works propose this approach to generate prescription maps and address focused local treatments [32]. In this work a K-means clustering was performed, asking for 3 clusters, for both $NDVI_{MS2}$ and $NDVI_{S2}$. Results were interpreted as the spatial basis to define prescription maps on. Since in a cluster analysis class meaning is not a-priori known, to recover it, NDVI mean and standard deviation were computed for all clusters for both the maps. After interpretation, a transition matrix was computed to test consistency of results.

3 Results and Discussions

3.1 MAIA S2 Calibration

The image block bundle adjustment accuracy using LOO procedure resulting in $RMSE_{x,y}$ and $RMSE_z$ equal to 0.39 m and 0.03 m respectively (Table 2). These accuracies well fits the TA requirements [33, 34], allowing fine spatially spectral measures of crops.

Table 2. GCP errors. For each GCP, reported values are those obtained during LOO when the considered GCP was excluded from bundle adjustment.

GCP ID	East err. (m)	North err. (m)	Height err. (m)	Total err. (m)	Projections	Error (# pixel)
1	0.248	0.239	−0.034	0.346	2	0.002
2	0.196	0.014	0.005	0.196	7	0.038
3	0.011	−0.443	0.022	0.445	6	0.008
4	−0.383	0.250	0.003	0.458	14	0.010
5	0.108	−0.433	0.044	0.449	3	0.007
6	−0.178	0.374	−0.045	0.416	8	0.018

3.2 Comparing MS2 and S2 Data

Band Correlation. Figure 3 and Table 3 show, for a I order polynomial regression model, the correspondent gain (α), offset (β), Pearson's *r* and coefficient of determination (R^2) values obtained from the comparison between MS2 and S2 datasets.

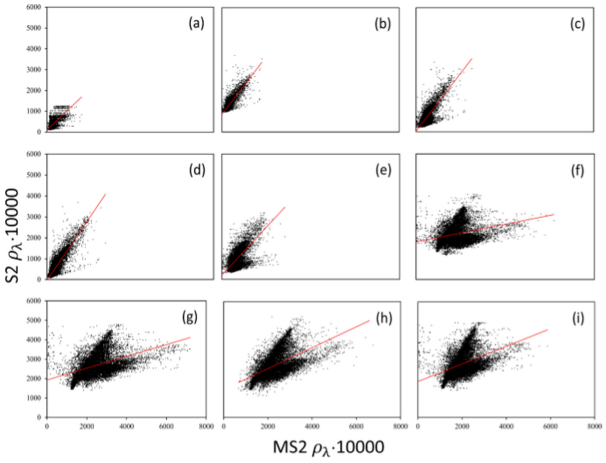


Fig. 3. I order polynomial regression models obtained comparing MS2 and S2 bands. (a) b1, (b) b2, (c) b3, (d) b4, (e) b5, (f) b6, (g) b7, (h) b8, (i) b8a.

Table 3 shows that compared bands provide different values of r and R^2. in particular, high values of r and R^2 were observed for visible bands (b2, b3 and b4), while red-edge and infrared bands (b6, b7 and b8) showed lower value.

3.3 Spectral Signature Assessment

Figure 4 shows RM and MM with the corresponding histograms as related to the spectral signature assessment.

Table 3. Slope (α), offset (β), correlation (r) and determination (R^2) values obtained comparing MS2 and S2 datasets. In red high values of r and R^2, in blue low values.

MAIA S2 and S-2 bands	r	α	β	R^2
b1	0.70	101.8876	0.9504	0.49
b2	0.88	-7.2242	1.6316	0.77
b3	0.79	25.4228	1.3984	0.63
b4	0.91	-27.9461	1.4640	0.83
b5	0.68	207.0060	1.1493	0.46
b6	0.27	1804.1660	0.2102	0.07
b7	0.43	1930.6425	0.3039	0.19
b8	0.55	1448.5376	0.5419	0.31
b8a	0.42	1867.7151	0.4572	0.18

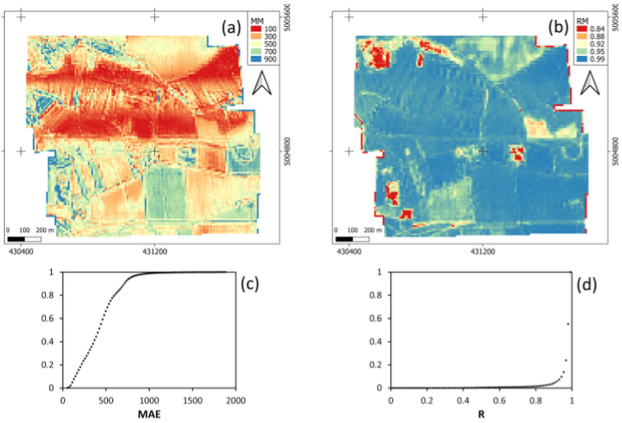


Fig. 4. (a) MM, (b) RM (c) cumulative frequency graph of MAE, (d) cumulative frequency graph of correlation. Reference system is WGS 84 UTM zone 32 N, EPSG: 32632.

In general, correlation between MS2 and S2 spectral signatures was always greater than 0.8, while MAE was lower than 600 in the 80% of the pixels. Nevertheless, some critical errors persist. Unexpectedly, MM and RM show a peculiar distribution over the scene. In particular, *r* and MAE values were lower in bare soils/built-up areas and where radiometric borders were present.

3.4 Vegetation Index Comparison

$NDVI_{MS2}$ and $NDVI_{S2}$ maps are reported in Fig. 5. The F-test proved that $NDVI_{MS2}$ and $NDVI_{S2}$ were significantly different ($F = 1.424$, $p < 0.001$) and $NDVI_{S2}$ variance was greater than $NDVI_{MS2}$ one, supporting the hypothesis that, in spite of the higher

resolution, MS2 can detect a lower NDVI variability than S2. Figure 5c reports NDVI difference. It shows that the majority of differences were located in bare soils, roads and built-up areas while, in the vegetated areas, differences were lower than 0.02. According to Borgogno et al. [35] these differences are not significant considering the NDVI uncertainty. To further explore NDVI differences a I order polynomial regression model was calibrated with reference to the scatterplot (Fig. 6) relating NDVI images (parameters are reported in Table 4).

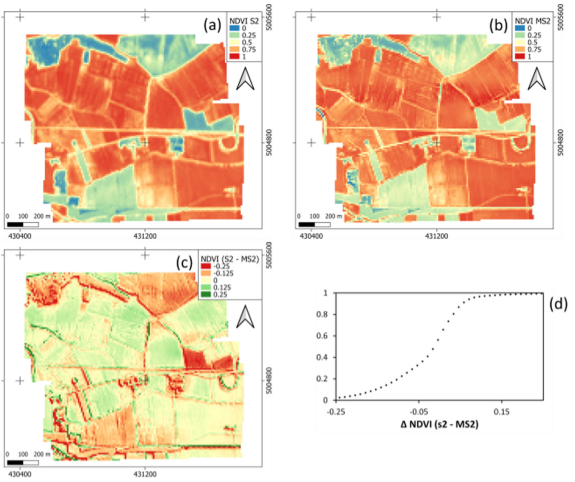


Fig. 5. (a) $NDVI_{S2}$ maps, (b) $NDVI_{MS2}$ map, (c) NDVI difference map, (d) Cumulative frequency histogram of NDVI difference map. Reference system is WGS 84 UTM zone 32 N, EPSG: 32632.

Table 4. Ordinary least squares regression between MS2 and S2 NDVI

Gain	1.1251
Offset	−0.1128
r	0.943
R^2	0.889
t	348.440
p-value	<0.001

Gain and offset values reported in Table 4 (1.125 and −0.11 respectively) suggest that MS2 tends to overestimate NDVI (with respect to S2). Overestimation reduces while NDVI value increases. With reference to the existence range of NDVI [−1.00, + 1.00], it can be noticed that the maximum overestimation value (about +0.24) occurs at $NDVI_{MS2} = -1.00$. Oppositely, the two measures can be retained as consistent when the difference between S2 NDVI and its estimation from MS2 is greater than 0.74.

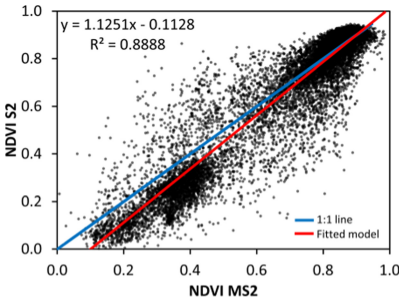


Fig. 6. Scatterplot and calibrated I order polynomial model relating MS2 and S2 NDVI maps.

These results raise some doubts about the consistency between aerial and satellite based remote sensing in precision agriculture and suggests that some questions, concerning their integration, remain open.

3.5 Effects of Datasets Spectral Inconsistencies on Prescription Maps

To test the effects of NDVI spectral inconsistencies a K-means clustering (3 clusters and 100 iterations) was run aimed at deriving the correspondent prescription maps (Fig. 7).

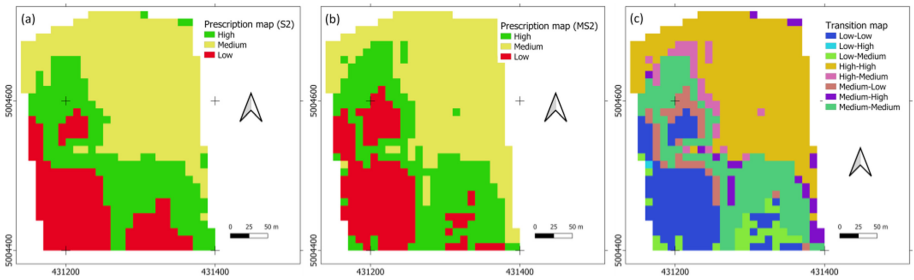


Fig. 7. (a) K-means clustering for $NDVI_{MS2}$, (b) K-means clustering for $NDVI_{S2}$, (c) transition map. Reference system is WGS 84 UTM zone 32 N, EPSG: 32632.

Meaning of classes was recovered considering their NDVI mean and standard deviation values (Fig. 8) assuming that "high", "medium" and "low" vigour classes were assigned with reference to the NDVI class mean values. A transition matrix (Table 5) and related map (Fig. 7c) were also computed by comparing the two obtained prescription maps. Results show that omission and commission errors range between 8 and 29% depending on the class. Higher commission values are related to low and medium vigour classes, i.e. where the most of spectral inconsistencies are placed according to the previously mentioned comparisons. The overall accuracy was found to be equal to 71%. These results suggest that MAIA and S2 sensors could drive to significantly different deductions while working with prescription maps involving vegetation spectral indices, where about 30% of pixels could be possibly assigned to different classes.

Table 5. Transition matrix between S2 and MS2 derived prescription maps.

		S2			
	(# pixels)	*Low*	*Medium*	*High*	Total
MS2	*Low*	131	36	0	167
	Medium	33	159	31	223
	High	1	24	299	324
	Total	165	219	330	714

(%)	Producer's Accuracy	User's Accuracy	Omission Error	Commission Error
Low	79.4	78.4	20.6	21.6
Medium	72.6	71.3	27.4	28.7
High	90.6	92.3	9.4	7.7
Overall Accuracy		70.8		

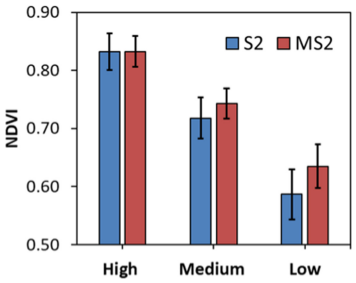


Fig. 8. Mean and standard deviation values of clusters generated by the K-means classification of $NDVI_{MS2}$ and $NDVI_{S2}$ maps.

4 Conclusions

In this work, MS2 and S2 radiometric consistency was assessed having comparable spectral bands. Assessment was aimed at testing if significantly different deductions could come from the adoption of the 2 sensors, with special concern about NDVI computation and its interpretation for prescription maps generation in the agriculture context. MS2 dataset was acquired by aerial survey and the subsequent radiometric and geometric calibration were performed following an ordinary workflow based on the MultiCam Stitcher Pro v 1.4-Beta 2 supplied with MAIA S2 sensor. Some potential weaknesses where preliminarily identified and highlighted concerning the data processing strategy implemented in the above mentioned software. MS2 was preliminarily downsampled from its native GSD down to S2 one (10 m). At the ground reflectance calibrated bands were compared at pixel level and showed a low correlation especially in the red-edge

and infrared bands ($r < 0.5$); differently, a high correlation was found for visible bands ($r > 0.8$). Moreover, MAE and r were also computed comparing, at pixel level, the local spectral signature of both multispectral stacks. Correlation resulted poor for bare soils/building areas and over radiometric borders. A further comparison was made focusing on NDVI maps from both the sensors, since it is widely used in precision agriculture. The analysis focused out that MS2 tends to overestimate NDVI values especially when working with values lower than 0.74. The difference increases while moving to lower values up to 0.23 when NDVI $= -1.00$. Results also showed that MS2 derived NDVI map presents a lower contrast if compared with the S2 one; this suggests a general a weakness of MS2 of appreciating NDVI differences. Based on these evidences a further analysis was performed for a focus area corresponding to a corn field to test possible effects in prescription maps as derivable from S2 and MS2 NDVI maps. Comparison highlighted commission/omission errors higher for low and medium vigour classes. This fact is consistent with the overestimation that was measured in the previous step. Finally, some doubts about the consistency between aerial and satellite based remote sensing in precision agriculture still persist, suggesting that some questions, concerning their integration, remain open. With these premises and considering cost related issues of aerial data, it appears to be desirable a further deepening concerning the reliability of spectral measures from airborne low cost sensors. Conversely, it is worth to remind that aerial surveys equipped with MS2 sensor can provide imagery having centimeter geometric resolution and 3D measurement potentialities that can be effectively used to improve crop related deductions.

References

1. Babaeian, E., et al.: others: A new optical remote sensing technique for high-resolution mapping of soil moisture. Front. Big Data **2**, 37 (2019)
2. Sishodia, R.P., Ray, R.L., Singh, S.K.: Applications of remote sensing in precision agriculture: A review. Remote Sens. **12**, 3136 (2020)
3. Monteleone, S., et al.: Exploring the adoption of precision agriculture for irrigation in the context of agriculture 4.0: the key role of internet of things. Sensors. **20**, 7091 (2020)
4. Borgogno-Mondino, E., Sarvia, F., Gomarasca, M.A.: Supporting insurance strategies in agriculture by remote sensing: a possible approach at regional level. In: Misra, Sanjay, Gervasi, Osvaldo, Murgante, Beniamino, Stankova, Elena, Korkhov, Vladimir, Torre, Carmelo, Rocha, Ana Maria A C., Taniar, David, Apduhan, Bernady O., Tarantino, Eufemia (eds.) ICCSA 2019. LNCS, vol. 11622, pp. 186–199. Springer, Cham (2019). https://doi.org/10.1007/978-3-030-24305-0_15
5. Sarvia, F., De Petris, S., Borgogno-Mondino, E.: Remotely sensed data to support insurance strategies in agriculture. In: Remote Sensing for Agriculture, Ecosystems, and Hydrology XXI, p. 111491H. International Society for Optics and Photonics (2019)
6. Sarvia, F., De Petris, S., Borgogno-Mondino, E.: Multi-scale remote sensing to support insurance policies in agriculture: from mid-term to instantaneous deductions. GISci. Remote Sens. **57**, 770–784 (2020). https://doi.org/10.1080/15481603.2020.1798600
7. De Petris, S., Sarvia, F., Borgogno-Mondino, E.: A new index for assessing tree vigour decline based on sentinel-2 multitemporal data. Application to tree failure risk management. Remote Sens. Lett. **12**(1), 58–67 (2020)

8. De Petris, S., Sarvia, F., Borgogno-Mondino, E.: RPAS-based photogrammetry to support tree stability assessment: Longing for precision arboriculture. Urban Forest. Urban Green. **55**, 126862 (2020). https://doi.org/10.1016/j.ufug.2020.126862
9. Sarvia, F., Xausa, E., Petris, S.D., Cantamessa, G., Borgogno-Mondino, E.: A possible role of copernicus sentinel-2 data to support common agricultural policy controls in agriculture. Agronomy **11**, 110 (2021)
10. Sarvia, F., De Petris, S., Borgogno-Mondino, E.: A methodological proposal to support estimation of damages from hailstorms based on copernicus sentinel 2 data times series. In: Gervasi, O., et al. (eds.) ICCSA 2020. LNCS, vol. 12252, pp. 737–751. Springer, Cham (2020). https://doi.org/10.1007/978-3-030-58811-3_53
11. De Petris, S., Sarvia, F., Gullino, M., Tarantino, E., Borgogno-Mondino, E.: Sentinel-1 polarimetry to map apple orchard damage after a storm. Remote Sens. **13**, 1030 (2021). https://doi.org/10.3390/rs13051030
12. De Petris, S., Sarvia, F., Borgogno-Mondino, E.: Multi-temporal mapping of flood damage to crops using sentinel-1 imagery: a case study of the Sesia River (October 2020), (2021)
13. Sarvia, F., De Petris, S., Borgogno-Mondino, E.: Exploring climate change effects on vegetation phenology by MOD13Q1 data: the Piemonte region case study in the period 2001–2019. Agronomy **11**, 555 (2021). https://doi.org/10.3390/agronomy11030555
14. Orusa, T., Orusa, R., Viani, A., Carella, E., Borgogno Mondino, E.: Geomatics and EO data to support wildlife diseases assessment at landscape level: a pilot experience to map infectious Keratoconjunctivitis in Chamois and phenological trends in Aosta Valley (NW Italy). Remote Sens. **12**, 3542 (2020)
15. van Klompenburg, T., Kassahun, A., Catal, C.: Crop yield prediction using machine learning: a systematic literature review. Comput. Electron. Agric. **177**, 105709 (2020)
16. Lessio, A., Fissore, V., Borgogno-Mondino, E.: Preliminary tests and results concerning integration of Sentinel-2 and Landsat-8 OLI for crop monitoring. J. Imaging **3**, 49 (2017)
17. Nocerino, E., Dubbini, M., Menna, F., Remondino, F., Gattelli, M., Covi, D.: Geometric calibration and radiometric correction of the MAIA multispectral camera. Int. Arch. Photogramm. Remote Sens. Spatial Inf. Sci. **42**(3), 149–156 (2017)
18. Marinello, F.: Last generation instrument for agriculture multispectral data collection. Agric. Eng. Int. CIGR J. **19**, 87–93 (2017)
19. Boccardo, P., Mondino, E.B., Tonolo, F.G.: High resolution satellite images position accuracy tests. In: IGARSS 2003. 2003 IEEE International Geoscience and Remote Sensing Symposium. Proceedings (IEEE Cat. No. 03CH37477), pp. 2320–2322. IEEE (2003)
20. Mondino, E.B., Perotti, L., Piras, M.: High resolution satellite images for archeological applications: the Karima case study (Nubia region, Sudan). Eur. J. Remote Sens. **45**, 243–259 (2012)
21. Ryan, C.G., et al.: MAIA mapper: high definition XRF imaging in the lab. J. Instrum. **13**, C03020 (2018)
22. Segarra, J., Buchaillot, M.L., Araus, J.L., Kefauver, S.C.: Remote sensing for precision agriculture: sentinel-2 improved features and applications. Agronomy **10**, 641 (2020)
23. Maggiore, P., Greco, A.: Development of the SmartGimbal Control System for the SmartBay Platform (2019).
24. Gascon, F., Cadau, E., Colin, O., Hoersch, B., Isola, C., Fernández, B.L., Martimort, P.: Copernicus sentinel-2 mission: products, algorithms and Cal/Val. In: Earth Observing Systems XIX, p. 92181E. International Society for Optics and Photonics (2014)
25. Dechoz, C., et al.: Sentinel 2 global reference image. In: Image and Signal Processing for Remote Sensing XXI, p. 96430A. International Society for Optics and Photonics (2015)
26. Borgogno-Mondino, E.: Remote sensing from RPAS in agriculture: an overview of expectations and unanswered questions. In: Ferraresi, C., Quaglia, G. (eds.) RAAD 2017. MMS, vol. 49, pp. 483–492. Springer, Cham (2018). https://doi.org/10.1007/978-3-319-61276-8_51

27. Brovelli, M.A., Crespi, M., Fratarcangeli, F., Giannone, F., Realini, E.: Accuracy assessment of high resolution satellite imagery orientation by leave-one-out method. ISPRS J. Photogramm. Remote. Sens. **63**, 427–440 (2008)
28. Lanaras, C., Bioucas-Dias, J., Galliani, S., Baltsavias, E., Schindler, K.: Super-resolution of Sentinel-2 images: learning a globally applicable deep neural network. ISPRS J. Photogramm. Remote. Sens. **146**, 305–319 (2018)
29. Willmott, C.J., Matsuura, K.: Advantages of the mean absolute error (MAE) over the root mean square error (RMSE) in assessing average model performance. Climate Res. **30**, 79–82 (2005)
30. Chauhan, S., et al.: Wheat lodging assessment using multispectral UAV data. Int. Arch. Photogramm. Remote Sens. Spatial Inf. Sci. **42**, 235–240 (2019)
31. Gómez-Candón, D., López-Granados, F., Caballero-Novella, J.J., Peña-Barragán, J.M., García-Torres, L.: Understanding the errors in input prescription maps based on high spatial resolution remote sensing images. Precision Agric. **13**, 581–593 (2012). https://doi.org/10.1007/s11119-012-9270-9
32. Bates, T., Dresser, J., Eckstrom, R., Badr, G., Betts, T., Taylor, J.: Variable-rate mechanical crop adjustment for crop load balance in "Concord" vineyards. In: Presented at the 2018 IoT Vertical and Topical Summit on Agriculture - Tuscany, IOT Tuscany 2018 (2018). https://doi.org/10.1109/IOT-TUSCANY.2018.8373046
33. Borgogno-Mondino, E., Lessio, A., Tarricone, L., Novello, V., de Palma, L.: A comparison between multispectral aerial and satellite imagery in precision viticulture. Precision Agric. **19**(2), 195–217 (2017). https://doi.org/10.1007/s11119-017-9510-0
34. Rokhmana, C.A.: The potential of UAV-based remote sensing for supporting precision agriculture in Indonesia. Procedia Environ. Sci. **24**, 245–253 (2015)
35. Borgogno-Mondino, E., Lessio, A., Gomarasca, M.A.: A fast operative method for NDVI uncertainty estimation and its role in vegetation analysis. Eur. J. Remote Sens. **49**, 137–156 (2016)